Strengthening and toughening mechanisms of an ultrafine grained Mg-Gd-Y-Zr alloy processed by cyclic extrusion and compression

Qudong Wang[a], *, Yongliang Mu[a], Jinbao Lin[b], Li Zhang[a], Hans J. Roven[c]

[a] National Engineering Research Center of Light Alloy Net Forming and State Key Laboratory of Metal Matrix Composites, Shanghai Jiao Tong University, Shanghai 200240, China

[b] School of Applied Science, Taiyuan University of Science and Technology, Taiyuan 030024, China

[c] Department of Materials Science and Engineering, Norwegian University of Science and Technology, Trondheim 7491, Norway

Abstract:

Cyclic extrusion and compression (CEC) was implemented to process the Mg-Gd-Y-Zr alloy. Microstructure characters, including the matrix grain, precipitates and texture evolution, were tried to correlate with the mechanical performance of the post-processed alloy. Results show that simultaneous improvements in the ductility and strength of Mg-Gd-Y-Zr alloy were achieved after CEC. Combination of the greatly refined matrix grain, uniformly precipitated nanoscale particles and gradually disintegrated texture should be responsible for this result. Besides, introducing of rare-earth elements was found to change the deformation mechanisms of the Mg alloy by facilitating non-basal slip systems, twinning and shear bands. This may further contribute to the enhanced mechanical properties.

Key words: Magnesium alloys; Ductility; Texture; Cyclic extrusion compression

*Corresponding author at: National Engineering Research Center of Light Alloy Net Forming and State Key Laboratory of Metal Matrix Composites, Shanghai Jiao Tong University, Shanghai 200240, China. Tel.: +86 21 54742715; Fax: +86 21 34202794.

E-mail address: wangqudong@sjtu.edu.cn (Q. D. Wang)

1. Introduction

The attainment of both strong and ductile Mg alloys is of considerable interest at present. However, due to the inherent hexagonal close-packed (hcp) structure, Mg and Mg alloys have limited number of independent slip systems, which leads to poor ductility and formability at room temperature [1, 2]. Thus, the microstructural optimization is of critical importance for Mg alloys to improve their formability and mechanical performances. It has been reported that an ultrafine-grained (UFG) structure prepared by severe plastic deformation (SPD) generally exhibits a superior strength than its coarse-grained counterpart [3-10]. However, the UFG alloys often have a very low or no work-hardening rate, which results in a low uniform elongation (strain before necking) under tensile stress. Recently, great efforts have been made to improve the ductility and strength of Mg alloys. It has been demonstrated that the ductility of Mg alloys can be enhanced by texture control and grain refinement [10-14]. Meanwhile, it was suggested that the increased cold formability of several Mg alloys, such as Mg-Ce, Mg-Li and Mg-Y, could be attributed to the introduction of the rare-earth (RE) elements [15-17]. More research indicated that the dislocation configuration, shear bands, random texture and recrystallization were associated with the RE in RE-containing magnesium [18-21]. Cyclic extrusion and compression (CEC) method is one of the continuous SPD processing. It imposes three dimensional compression stresses, which is favorable to process the hard-to-deform Mg alloy [4, 22]. On the other hand, the addition of RE is also necessary for increased formability of Mg alloy in terms of the formation of shear bands, which were suggested to act as "softening" regions. We have already found considerable shear bands in Mg-Gd-Y-Zr (GW102K) alloy during the processing [5], which is in accordance with the results of Ref. [20, 23]. In the present work, CEC processing was applied to a RE-containing GW102K Mg alloy in order to refine grains. The study focuses on determining the correlation between the microstructure and deformation behaviors of GW102K alloy. The effects of precipitation phase and texture on the ductility are also considered.

2. Materials and methods

The initial alloy used in this study was Mg-9.95wt.%Gd-2.3wt.%Y-0.46wt.%Zr alloy (designed as GW102K). For comparison, a commercial ZK60 (Mg-5.5wt.%Zn-0.5 wt.%Zr) alloy was also investigated. The initial GW102K alloy was received in the form of an extruded bar with a diameter of 29.5 mm and then cut into pieces of length 42 mm before cyclic extrusion and compression (CEC). The operation procedure of CEC method was described elsewhere [4, 24]. The temperature for CEC processing was designed as 350 °C, 400 °C and 450 °C. It needs to be emphasized that the number of extrusion passes was

defined as the number of specimen passes through the die. At the final pass, one ram was removed so that the other ram could extrude the specimen to a rod of 20 mm in diameter. Microstructure and texture were investigated by electron backscattered diffraction (EBSD) in a Zeiss 55VP FEG-SEM equipped with a Nordif EBSD detector and the TSL OIM EBSD software. All measurements were taken along the longitudinal section of the processed materials. Tensile specimens with a gauge length of 10 mm were spark machined out of the rods along the longitudinal section. Tensile tests were performed at room temperature with an initial strain rate of 5×10^{-3} s^{-1}.

The average grain size of the GW102K alloy before CEC processing and after 4, 8 as well as 14 passes (450 °C) have been determined to be ~20 μm, ~3.5 μm, ~2.2 μm and ~1 μm, respectively [5]. After 4 and 8 passes, the grains were clearly refined to ultrafine-size and became fairly homogeneous due to the occurrence of dynamic recrystallization (DRX) during the deformation process. The grain boundary statistics from EBSD measurement indicated that the fraction of high angle grain boundaries (HAGBs, with misorientation angle above 15°) for the GW102K alloy after 4, 8 and 14 passes (350-450 °C) were over 93%. Meanwhile, the CECed-sample exhibited a random distribution of misorientation angles, without any preferential peaks.

3. Results and discussion

In the present work, the processing temperature is above 300 °C. Thus, the precipitation is inevitable during the extrusion and CEC processing. Fig.1 shows a high density of second-phase particles with an average size range of ~100-200 nm in CEC-ed GW102K alloy at 450 °C. In general, high-temperature aging for Mg-Gd-Y-Zr alloy (>400 °C) may lead to coarse precipitation particles located at the grain boundaries. Fig.1a, however, indicated some nanoscale spherical precipitation particles located at grain boundaries as well as partial within grain interiors. It seems that the coarse second-phase particles were crushed during CEC processing. Two refining modes of secondary-phase particles referred to as tension tearing and shearing fracture were observed, which were shown in Fig.1b and Fig.1c. The X-ray diffraction (XRD) pattern illustrated that these second-phase particles, for the most part, were $Mg_{24}(Gd,Y)_5$. Other phases such as $Mg_{24}Y_5$ and Mg_5Gd were existed at less than 0.1%.
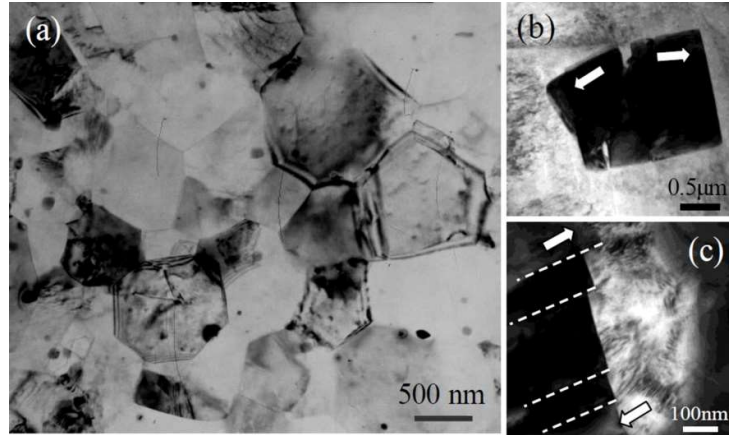
Fig.1: TEM photographs for the distribution and refining mechanism of precipitation particles in GW102K alloy: (a) after 14 passes CEC at 450 °C; (b) particle fracture due to tension and (c) tearing due to shearing.

We have determined that the as-extruded GW102K alloy exhibited a fiber texture of (ED∥<$10\bar{1}0$>) [22]. A similar texture (i.e. {0002} basal planes lying parallel to the extrusion direction) was observed in the extruded ZK60 Mg alloy [4]. After CEC processing, the initial fiber texture became disintegrated and a new $\{10\bar{1}3\} < 30\bar{3}2 >$ $+\{10\bar{1}1\} < 1\bar{5}43 >$ type texture was presented. However, the maximum texture intensities for the over 2 passes CEC processed GW102K alloy were below 2.5, meaning that the grain orientations were still very random. According to the {0002} pole figures of GW102K alloy before and after CEC in Ref. [5], the quantitative texture analysis was performed by investigating {0002} pole plot calculated from the {0002} pole figures. Fig.2 shows the {0002} plane orientation concentration of GW102K and ZK60 (inserted) alloy before and after CEC. It is obvious that, for both alloys, the pole intensity decreased. The maximum pole density area deviated from the pole equator was 20-30° for the CECed ZK60 alloy, however, 20-60° for the CECed GW102K alloy. The texture concentration of GW102K alloy is much lower than that of ZK60 alloy. For the as-extruded GW102K alloy, 46.6% of the {0002} planes were orientated below 20° with respect to the extrusion axis. However, the fraction is 85% for as-extruded ZK60 alloy, indicating a high degree of fiber texture concentration. After CEC, the distribution of {0002} pole density for GW102K alloy is more even without prominent peaks, indicating a more random grain orientation. Thus, the quantitative texture analysis before and after CEC illustrated that CEC processing not only refined the matrix grains, but weaken the initial fiber texture.
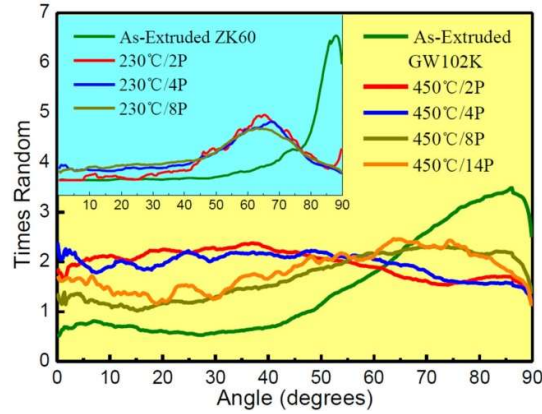
Fig.2: Effects of CEC pass number on the {0002} pole plot of GW102 alloy calculated from {0002} pole figure.

Effects of CEC parameters on the ultimate tensile strength (UTS), yield strength (YS) and elongation-to-fracture (Elongation) of GW102K alloy were presented in Fig.3a, Fig.3b and Fig.3c, respectively. The increase in CEC pass number means the decrease in grain size [4]. Two unusual features for the properties can be observed: (I) YS tends to rise as the CEC pass number increases; (II) Elongation simultaneously increases considerably though the grains were clearly refined to ultra-fine size.
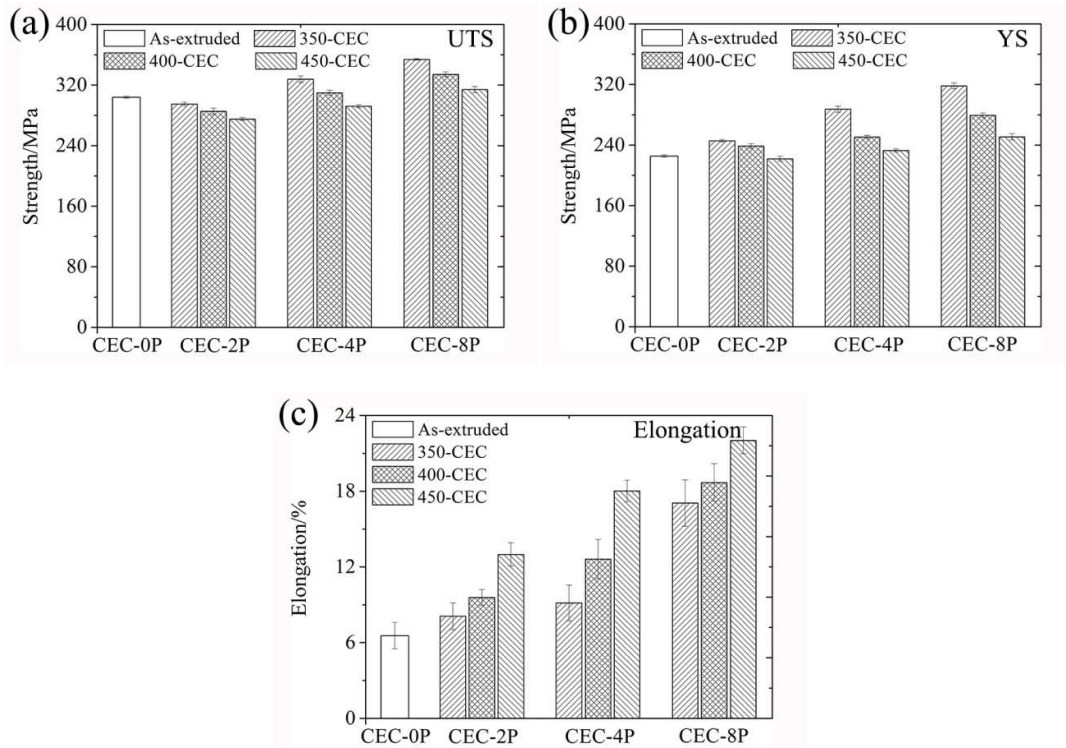

Fig.3: Effect of CEC deformation pass number on the tensile properties: (a) ultimate tensile strength (UTS); (b) yield strength (YS); (c) Elongation to fracture (Elongation).

First, according to Hall-Petch (H-P) relation, a rise in YS with the decreasing of grain size is reasonable. However, the inverse H-P effect was observed at ultra-fine-grain size in many Mg alloys processed by SPD [11-14]. Especially, we have also demonstrated that the YS of ZK60 Mg alloy decreased after 2-pass and 4-pass CEC [4], which is quite different from the observed increasing in YS for CECed GW102 alloy. The relationships between YS and the inverse square root of the grain size for both GW102K and ZK60 alloy are shown in Fig.4. Most of the models proposed to explain the inverse H-P behavior for nanocrystalline materials such as Cu and Ni fall into at least one of four categories, namely dislocation-based models, diffusion-based models, rain-boundary-shearing models and two-phase-based models [25]. The texture change of Mg alloy during SPD processing, however, was thought to be responsible for the deviation from the H-P relation [4, 10, 13]. The occurrence of normal H-P effect is unnatural for CECed GW102K alloy. We believe that the phenomenon is associated with the texture as well as the nanoscale second-phase particles. It has been demonstrated that the softening, resulting from the rising in Schmid factor (SF) on the basal slip system due to the deviations from the ideal $<10\bar{1}0>$ fiber texture, was a principal cause for the decreasing in YS for ZK60 alloy after 2-pass and 4-pass CEC [4]. For GW102K alloy, the difference of texture intensity between as-extrusion sample and CECed sample was much smaller than that of ZK60 alloy (see Fig.2). Thus, it suggests that the lower initial texture intensity for as-extrusion GW102K alloy and smaller intensity difference before and after CEC can account for the rising in YS for CECed GW102K alloy. On the other hand, the nanoscale second-phase precipitation, as a strengthening mechanism to block the motion of the dislocations, also contributes to the YS.
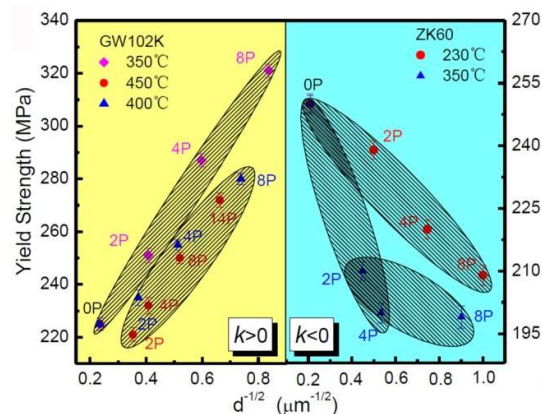

Fig.4: 0.2% proof stress of CECed-GW102K and CECed-ZK60 alloy as a function of $d^{-1/2}$.

Second, it is well known that UFG metals/alloys produced by SPD usually have high

strength but relatively low ductility at ambient temperatures. The CECed GW102K alloy, however, exhibited a considerable increase in elongation, elongation increased by 200-400% after 4-14 passes CEC at 450 °C, and 40-170% after 4-8 passes CEC at 350 °C. Fig.5 shows the fracture surface of tensile specimens before and after CEC. The fracture surface is occupied by plenty of dimples for the CECed-specimen (450 °C/8P, Fig.5b), showing higher ductility than the as-extruded specimen. The CEC processing seems favorable for improving the ductility of GW102K alloy.

It has been identified that the texture weakening owing to CEC processing resulted in a high activity of the basal slip owing to the rising in SF. On the other hand, the transition of deformation mechanisms from primary <a> basal slip and $\{10\bar{1}2\}<10\bar{1}1>$ tensile twin to <a> basal plus <c+a> pyramidal slip and secondary twinning caused a homogeneous deformation with enhanced ductility, which was attributed to the introduction of RE elements (Gd and Y) [17, 26]. The microstructures at the regions adjacent to the fracture surface of tensile specimens before and after CEC were shown in Fig.5c and d. Twin and shear bands were observed in both specimens. In as-extrudes specimen, high strain appears in a few narrow band-like structures, which carries more strain than other areas. In contrast, in the CECed specimen, large amounts of band-like structures are approximately homogeneously distributed over the observed area, indicating a homogeneously deformation with few local strain concentration. Thus, we concluded that shear bands in GW102K alloy are a significant cause for the enhanced room temperature ductility. Another factor that improves the ductility of CECed GW102K alloy may be the grain boundary sliding. As shown in Fig.5c and d, most grains keep equiaxed (not fibrillar) at regions adjacent to fracture surface. Further study, certainly, is needed to identify the contribution of grain boundary sliding on the enhanced ductility. Twinning was still found inevitable in tension even for UFG GW102K specimens. In CECed GW102K alloy, plenty of tiny tensile twins are observed and secondary twins are also present (Fig.5b), hinting that twinning remains a significant deformation mechanism for UFG GW102K alloy. Misorientation map of tensile specimens at regions adjacent to fracture surface was also shown in Fig.5e and f. For both as-extruded and CECed specimens, the number fraction of low angle grain boundary shows a sharp increase, indicating plenty of <a> and <c+a> slip. In addition, distinguished boundary misorientation peaks in the range 30-40° and ~85-90° were also observed. Combining the twin distribution in Fig.5c and d as well as the previously reported results [27, 28], it was confirmed that the local peak in the range ~85-90° can be ascribed to the $\{10\bar{1}2\}<10\bar{1}1>$ tensile twin. Also, the peaks in the range 30-40° were related to $\{10\bar{1}1\}\{10\bar{1}2\}$ double twins. The frequencies of

boundary misorientation peaks in the range 30-40° and ~85-90° (Fig.5e and f) for CECed specimen were higher than that of as-extruded specimen, indicating more tensile twins and secondary twins. It corresponds to the results on twins in Fig.5c and d.
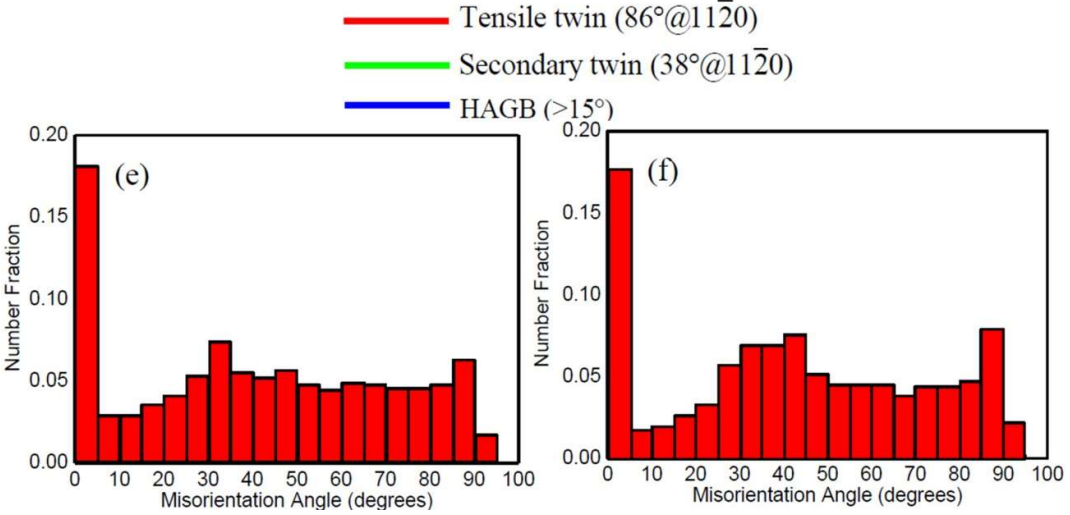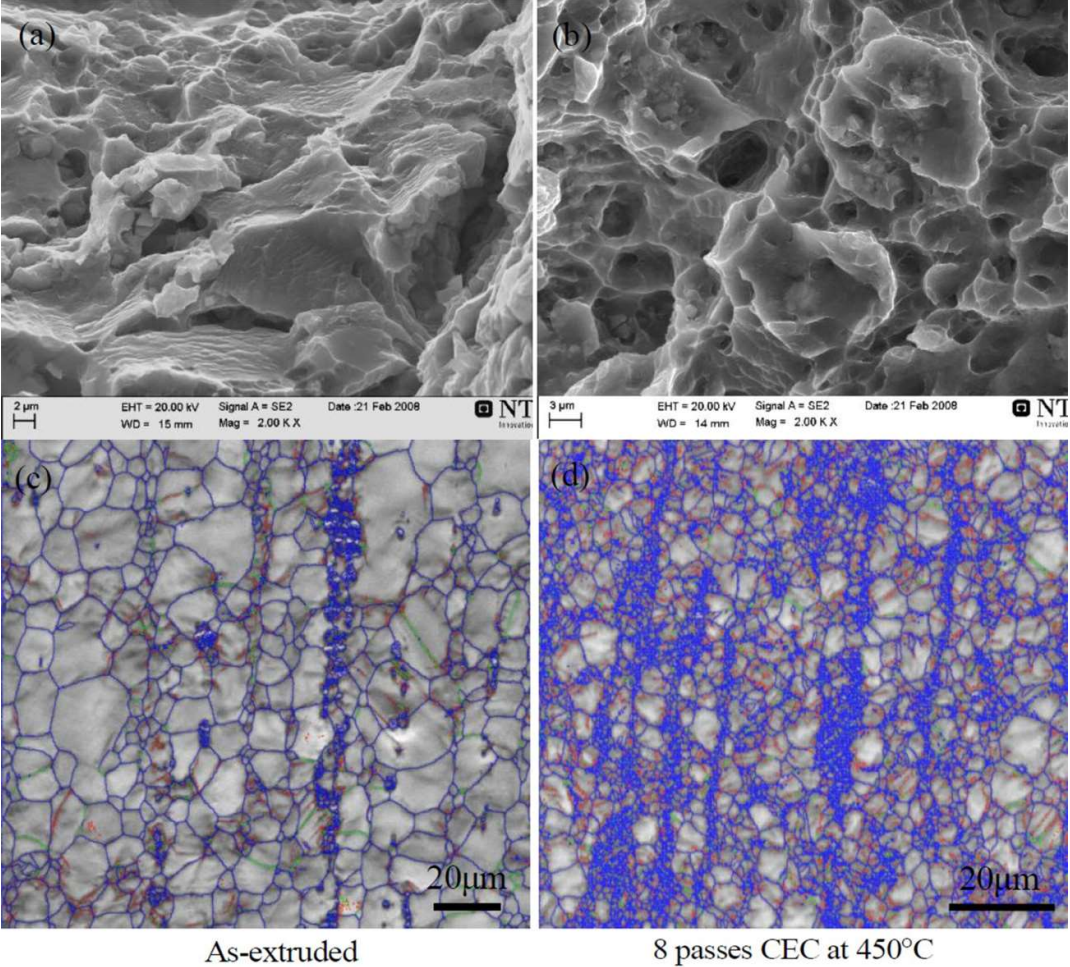

Fig.5: SEM morphology of fracture surfaces of tensile specimens before and after CEC

processing (a) as-extruded, (b) CEC 450 °C/8P; Grain boundaries and twin distribution at regions adjacent to fracture surface of tensile specimens (c) as-extruded, (d) CEC 450 °C/8 passes; Misorientation map at regions adjacent to fracture surface of tensile specimens (e) as-extrued, ε=6.9, fracture, (f) 450 °C/8P, ε=21%, fracture.

4. Conclusions

In summary, this study presents a simultaneously increase in the ductility and strength of UFG GW102K alloy produced by CEC processing. Unlike AZ and ZK series alloys processed by SPD, CECed-GW102K alloy obeyed Hall-Petch effect. We suggest that ultrafine-grain size, texture weakening and nanoscale precipitation particles were responsible for both high ductility and high strength. Besides basal slip, pyramidal slip, twinning and shear bands were also the significant deformation mechanisms for GW102K alloy, which can be attributed to the introduction of RE elements. Finally, we anticipate the same processing strategy (CEC) and materials design (RE) can be successfully used to produce bulk UFG Mg alloy with high strength and good ductility that required in practical application.

References:

[1] A. Chapuis, J.H. Driver, Temperature dependency of slip and twinning in plane strain compressed magnesium single crystals, *Acta Mater.* 59(5) (2011) 1986-1994.

[2] H. Zhou, Q.D. Wang, B. Ye, W. Guo, Hot deformation and processing maps of as-extruded Mg–9.8Gd–2.7Y–0.4Zr Mg alloy, *Mater. Sci. Eng. A* 576(0) (2013) 101-107.

[3] S.R. Agnew, J.A. Horton, T.M. Lillo, D.W. Brown, Enhanced ductility in strongly textured magnesium produced by equal channel angular processing, *Scr. Mater.* 50(3) (2004) 377-381.

[4] J. Lin, Q. Wang, L. Peng, H.J. Roven, Microstructure and high tensile ductility of ZK60 magnesium alloy processed by cyclic extrusion and compression, *J. Alloy Compd.* 476(1–2) (2009) 441-445.

[5] T. Peng, Q. Wang, J. Lin, M. Liu, H.J. Roven, Microstructure and enhanced mechanical properties of an Mg–10Gd–2Y–0.5Zr alloy processed by cyclic extrusion and compression, *Mater. Sci. Eng. A* 528(3) (2011) 1143-1148.

[6] B. Mansoor, A.K. Ghosh, Microstructure and tensile behavior of a friction stir

processed magnesium alloy, *Acta Mater.* 60(13–14) (2012) 5079-5088.

[7] W.J. Kim, Y.G. Lee, M.J. Lee, J.Y. Wang, Y.B. Park, Exceptionally high strength in Mg–3Al–1Zn alloy processed by high-ratio differential speed rolling, *Scr. Mater.* 65(12) (2011) 1105-1108.

[8] M.T. Pérez-Prado, d. Valle, O.A. Ruano, Grain refinement of Mg–Al–Zn alloys via accumulative roll bonding, *Scr. Mater.* 51(11) (2004) 1093-1097.

[9] L. Zhang, B. Ye, W. Liao, H. Zhou, W. Guo, Q. Wang, H. Jiang, W. Ding, Microstructure evolution and mechanical properties of AZ91D magnesium alloy processed by repetitive upsetting, *Mater. Sci. Eng. A* 641 (2015) 62-70.

[10] W.Z. Chen, X. Wang, E.D. Wang, Z.Y. Liu, L.X. Hu, Texture dependence of uniform elongation for a magnesium alloy, *Scr. Mater.* 67(10) (2012) 858-861.

[11] T. Mukai, M. Yamanoi, H. Watanabe, K. Higashi, Ductility enhancement in AZ31 magnesium alloy by controlling its grain structure, *Scr. Mater.* 45(1) (2001) 89-94.

[12] H. Somekawa, T. Mukai, Fracture toughness in Mg–Al–Zn alloy processed by equal-channel-angular extrusion, *Scr. Mater.* 54(4) (2006) 633-638.

[13] W.J. Kim, S.I. Hong, Y.S. Kim, S.H. Min, H.T. Jeong, J.D. Lee, Texture development and its effect on mechanical properties of an AZ61 Mg alloy fabricated by equal channel angular pressing, *Acta Mater.* 51(11) (2003) 3293-3307.

[14] W.J. Kim, C.W. An, Y.S. Kim, S.I. Hong, Mechanical properties and microstructures of an AZ61 Mg Alloy produced by equal channel angular pressing, *Scr. Mater.* 47(1) (2002) 39-44.

[15] S.R. Agnew, M.H. Yoo, C.N. Tomé, Application of texture simulation to understanding mechanical behavior of Mg and solid solution alloys containing Li or Y, *Acta Mater.* 49(20) (2001) 4277-4289.

[16] M.H. Yoo, J.R. Morris, K.M. Ho, S.R. Agnew, Nonbasal deformation modes of HCP metals and alloys: Role of dislocation source and mobility, *Metall. Mater. Trans. A* 33(3) (2002) 813-822.

[17] S. Sandlöbes, S. Zaefferer, I. Schestakow, S. Yi, R. Gonzalez-Martinez, On the role of non-basal deformation mechanisms for the ductility of Mg and Mg–Y alloys, *Acta Mater.* 59(2) (2011) 429-439.

[18] H. Yan, S.W. Xu, R.S. Chen, S. Kamado, T. Honma, E.H. Han, Twins, shear bands and recrystallization of a Mg–2.0%Zn–0.8%Gd alloy during rolling, *Scr. Mater.* 64(2) (2011) 141-144.

[19] N. Stanford, Micro-alloying Mg with Y, Ce, Gd and La for texture modification—A comparative study, *Mater. Sci. Eng. A* 527(10–11) (2010) 2669-2677.

[20] L.W.F. Mackenzie, M.O. Pekguleryuz, The recrystallization and texture of magnesium–zinc–cerium alloys, *Scr. Mater.* 59(6) (2008) 665-668.

[21] H. Zhou, B. Ye, Q.D. Wang, W. Guo, Uniform fine microstructure and random texture of Mg-9.8Gd-2.7Y-0.4Zr magnesium alloy processed by repeated-upsetting deformation, *Mater. Lett.* 83 (2012) 175-178.

[22] J. Lin, X. Wang, W. Ren, X. Yang, Q. Wang, Enhanced Strength and Ductility Due to Microstructure Refinement and Texture Weakening of the GW102K Alloy by Cyclic Extrusion Compression, *J. Mater. Sci. Technol.* 32(8) (2016) 783-789.

[23] S.L. Couling, J.F. Pashak, L. Sturkey, Unique deformation and aging characteristics of certain magnesium-base alloys, *ASM-Trans* 51 (1959) 94-107.

[24] L. Zhang, Q. Wang, W. Liao, W. Guo, W. Li, H. Jiang, W. Ding, Microstructure and mechanical properties of the carbon nanotubes reinforced AZ91D magnesium matrix composites processed by cyclic extrusion and compression, *Mater. Sci. Eng. A* http://dx.doi.org/10.1016/j.msea.2017.02.076

[25] C.E. Carlton, P.J. Ferreira, What is behind the inverse Hall–Petch effect in nanocrystalline materials?, *Acta Mater.* 55(11) (2007) 3749-3756.

[26] S. Sandlöbes, M. Friák, S. Zaefferer, A. Dick, S. Yi, D. Letzig, Z. Pei, L.F. Zhu, J. Neugebauer, D. Raabe, The relation between ductility and stacking fault energies in Mg and Mg–Y alloys, *Acta Mater.* 60(6–7) (2012) 3011-3021.

[27] Y. Li, S. Wu, H. Bian, N. Tang, B. Liu, Y. Koizumi, A. Chiba, Grain refinement due to complex twin formation in rapid hot forging of magnesium alloy, *Scr. Mater.* 68(3–4) (2013) 171-174.

[28] L. Zhang, Q. Wang, W. Liao, W. Guo, B. Ye, W. Li, H. Jiang, W. Ding, Effects of cyclic extrusion and compression on the microstructure and mechanical properties of AZ91D magnesium composites reinforced by SiC nanoparticles, *Mater. Charact.* 126 (2017) 17-27.